DEUTSCHES ELEKTRONEN-SYNCHROTRON

DESY 93-077
June 1993

New Results from the H1 Experiment at HERA on Photoproduction, Deep Inelastic Scattering and Searches for New Particles

M. Erdmann
Deutsches Elektronen-Synchrotron DESY, Hamburg

H. Küster
III. Physikalisches Institut, RWTH Aachen

S. Levonian
Deutsches Elektronen-Synchrotron DESY, Hamburg
and
Lebedev Physical Institute, Moscow, Russia

Y. Sirois
LPNHE, Ecole Polytechnique, IN2P3-CNRS, Palaiseau, France

C. Vallee
LPNHE, Universités VI and VII, IN2P3-CNRS, Paris, France

ISSN 0418-9833

NOTKESTRASSE 85 - 22603 HAMBURG

To be sure that your preprints are promptly included in the
HIGH ENERGY PHYSICS INDEX,
send them to (if possible by air mail):

DESY **Bibliothek** **Notkestraße 85** **22603 Hamburg** **Germany**	**DESY-IfH** **Bibliothek** **Platanenallee 6** **15738 Zeuthen** **Germany**

DESY 93-077
June 1993

ISSN 0418-9833

New Results from the H1 Experiment at HERA on Photoproduction, Deep Inelastic Scattering and Searches for New Particles

presented at the *XXVIIIth Rencontres de Moriond*, Les Arcs, France, March 1993

by

M. Erdmann[2], H. Küster[1], S. Levonian[2,3], Y. Sirois[4] and C. Vallee[5]

[1] *III. Physikalisches Institut der RWTH, Aachen, Germany*
[2] *DESY, Hamburg, Germany*
[3] *Lebedev Physical Institute, Moscow, Russia*
[4] *LPNHE, Ecole Polytechnique, IN2P3-CNRS, Palaiseau, France*
[5] *LPNHE, Universités Paris VI and VII, IN2P3-CNRS, Paris, France*

LOW AND MEDIUM $p_\perp$ PHOTOPRODUCTION AT HERA

Sergey LEVONIAN
DESY, Hamburg, Germany / LPI, Moscow, Russia
H1 Collaboration

ABSTRACT

Quasi-real photoproduction has been studied in the H1 detector, based on the low Q^2 ep-scattering at HERA. Results are presented on measurements of the total photoproduction cross section, elastic ρ^0 production $\gamma p \to \rho^0 p$ and inclusive charged particle spectra in the central region from inelastic γp interactions. Although difficult to interpret theoretically, low and medium $p_\perp$ photoproduction processes nevertheless provide essential information for the understanding and complete description of γp interactions at high energies.

To appear in the proceedings of the session 'QCD and High Energy Hadronic Interactions'
(20-27 March 1993)

INTRODUCTION. It is well-known, that the photon is a pointlike gauge particle. Sometimes however, it can manifest itself as a complex object having an internal structure. This dual nature of the photon excites special interest in photoproduction physics. The recently commissioned electron-proton collider HERA in addition to its main task – measurement of deep inelastic scattering (DIS) – offers the possibility of studying photoproduction processes in a new energy domain compared with existed fixed target experiments. The bulk of the cross section is expected to be produced by soft photoproduction. Although they cannot be explained presently from first principles, these processes give important information on the complete description of γp interactions. So far the vector meson dominance model (VDM)[1] has been used to describe low $p_\perp$ photoproduction, while perturbative QCD pretends to explain high $p_\perp$ γp events. Matching between the two approaches is an important problem. Recently, a new and interesting attempt has been made to develop a combined description of soft and hard photoproduction at high energies[2]. The different scenarios presented there, including the whole concept used, can only be tested by confrontation with experimental data.

Thus, γp physics at HERA is potentially very fruitful. Below, first results on low and medium $p_\perp$ photoproduction are discussed, based on H1 data collected in 1992 at 26.7×820 GeV ep collision energy and corresponding to an integrated luminosity $\mathcal{L} \simeq 25$ nb^{-1}. Other interesting aspects of these data, related to the photoproduction of jets, have also been presented at this conference[3].

EVENT SELECTION. An important feature of the H1 detector and trigger design[4] is the possibility of keeping soft physics without affecting DIS and high $p_\perp$ photoproduction. This is by no means a trivial task, given the difficult background conditions at HERA. Most dangerous are proton-gas events in the ep interaction region which have a topology very similar to that of soft photoproduction events. The trigger for the minimum bias γp sample required a coincidence between signals from the H1 tracking system and the small angle electron tagger. The electron tagger is a part of the H1 luminosity monitor[4] and has an average acceptance of 35% for scattered electrons e' within the kinematical range $10^{-8} < Q^2 < 10^{-2}$ GeV^2 and $0.2 < y = 1 - E_{e'}/E < 0.8$. The events detected by such a trigger give a clean γp sample: the small amount of p-gas events appearing in random coincidence with the e' in the electron tagger, could be removed by further offline selections. Finally, the remaining background has been estimated to be less than 4% (2.2% from the p-gas and 1.6% from the e-gas events). The use of the electron tagger gives additional advantages: precise y (and thus $W_{\gamma p} = \sqrt{ys}$ at $Q^2 \to 0$) determination with an accuracy of (3-4)% and partial cancellation of the systematic error in the luminosity, related to the tagger acceptance ($\sigma_{\gamma p}^{tagged} \sim N_{\gamma p}/\mathcal{L} \sim A(\text{luminosity})/A(\gamma p)$). Most of the results presented are based on the e-tagged sample, exept for quasi-elastic ρ^0 production where the acceptance of the H1 tracking system for the decay pions does not overlap with that of the tagger for the scattered electron.

TOTAL γp CROSS SECTION. A comprehensive summary of the total photoproduction cross section status in pre-HERA days can be found in[5]. A large variety of models, predicting $\sigma_{tot}(\gamma p)$ values between 145 μb and 760 μb at 250 GeV centre of mass energy, allowed HERA to make an immediate and valuable contribution to γp physics at high energies.

First measurements of the γp total cross section at HERA by ZEUS[6] and H1[7] were based on small statistics of 0.2 nb^{-1} and 1.5 nb^{-1} respectively. Here a new H1 result is presented which is in agreement with the published one, but has somewhat smaller error. A detailed description of the method used can be found elsewhere[7].

Data sample	$E_{e'}$ [GeV]	$W_{\gamma p}$[GeV]	$\mathcal{L}$ [nb^{-1}]	$N_{\gamma p}$	$\sigma_{\gamma p}$ [μb]
July 1992	$10-19$	195	1.5 ± 0.1	917 ± 38	$159 \pm 7(stat) \pm 20(syst)$
Fall 1992	$5-22$	197	21.9 ± 1.5	16393 ± 174	$156 \pm 2(stat) \pm 18(syst)$

Compared to the summer period, better background conditions due to improved beam quality and trigger tuning allowed the use of the full acceptance of the electron tagger, and thus reduced systematics related to the tagger calibration precision. The dominant contributions to the systematic error are a 6% uncertainty in the luminosity measurement and 10% error in the detector acceptance determination. The energy dependence of the γp total cross section is shown in fig. 1. Regge motivated parametrizations are in good agreement with the data, while the extreme models predicting strong rise of $\sigma_{tot}(\gamma p)$[8] can be ruled out. More elaborated 'eikonalized' models[9] can describe $\sigma_{\gamma p}(s)$ better than those using a simple ansatz: $\sigma_{\gamma p}(s) = \sigma^{soft} + \sigma^{jet}(s)$.

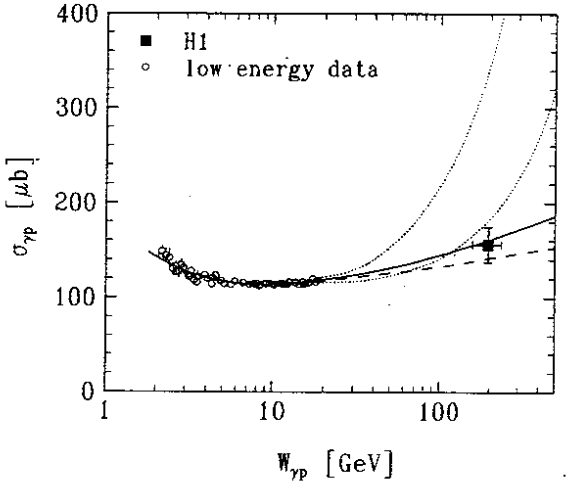

Figure 1: The energy dependence of the total γp cross section. The solid curve represents a Regge motivated fit of low energy data[10]. The dashed curve is the prediction of ALLM parametrization[11]. The dotted lines are obtained in the PYTHIA Monte Carlo[12] using the anzatz $\sigma_{\gamma p}(s) = \sigma^{soft} + \sigma^{jet}(s)$ with the Drees-Grassie parametrization of the photon structure function for $\hat{p}_t^{min} = 1.4$ GeV/c (upper line) and for $\hat{p}_t^{min} = 2.0$ GeV/c (lower line).

ELASTIC ρ^0 PRODUCTION. The study of elastic photoproduction of vector mesons, $\gamma p \to Vp$, in H1 relies mainly on the tracking system. Well measured 2-prong events with vertex position $|z_0| < 50$ cm have been selected, where the two charged particles in the final state were identified as pions or kaons by their dE/dx in the central jet chamber. The inelastic (and partially diffractive) components were suppressed by requiring no activity in the calorimeters, except for areas of possible small energy deposit from the vector meson decay products. The acceptance of the tracking chambers limited the available energy range of the elastic ρ^0 production to the $20 < W_{\gamma p} < 80$ GeV. This interval has been subdivided into two W-bins with approximately equal statistics: $W_{\gamma p} < 40$ GeV and $W_{\gamma p} > 40$ GeV. As an illustration, fig. 2 shows a nice ρ^0 signal in the $\pi^+\pi^-$ mass distribution for the high energy bin. $M_\rho = 769 \pm 7$ MeV has been obtained from the fit by the relativistic Breit-Wigner cross section modified by the phenomenological Ross-Stodolsky factor[13], accounting for the skewing of the ρ^0-signal shape. Some indication of elastic φ production (10±3 events) is also seen in the K^+K^- mass spectrum. Comparison with the Monte Carlo has shown, that the remaining contamination from the diffractive component in our elastic ρ^0 sample is less that 10% in the range of four-momentum transfer squared $|t| < 0.4$ GeV^2.

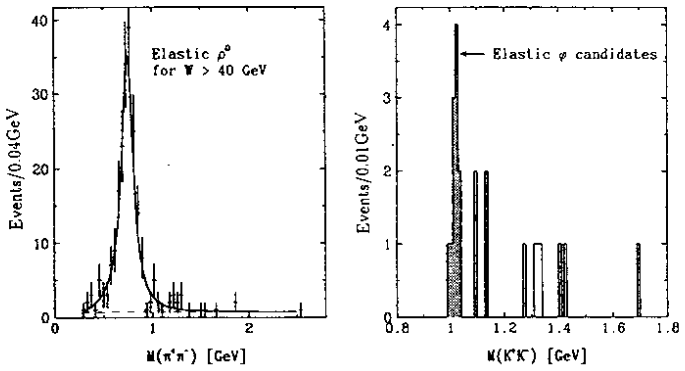

Figure 2: Signals of the elastic $\gamma p \to Vp$ scattering observed in the H1 detector

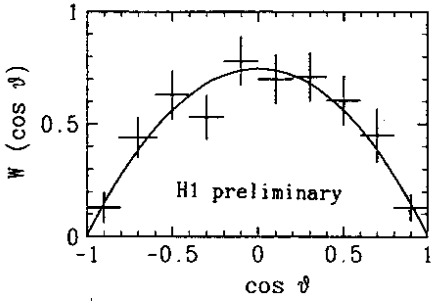

Figure 3: The angular distribution of the decay pions in the helicity frame.

The angular distribution of the decay pions (fig. 3) is in agreement with the $\sin^2\theta$ shape expected for transversly polarized photons at $Q^2 \to 0$ (in our sample the average value of $<Q^2>= 0.08$ GeV^2).

The slope of the t-distribution in the reaction $\gamma p \to \rho^0 p$ has been defined by fitting an exponent function e^{bt} to our data in the interval $|t| < 0.32$ GeV^2 (fig.4 a,b). The results for two energy intervals: $b = 9.4 \pm 1.1$ GeV^{-2} at $W_{\gamma p} = 20 - 40$ GeV and $b = 11.1 \pm 1.3$ GeV^{-2} at $W_{\gamma p} = 40 - 75$ GeV, are compared to the low energy data[13] in fig. 4c.

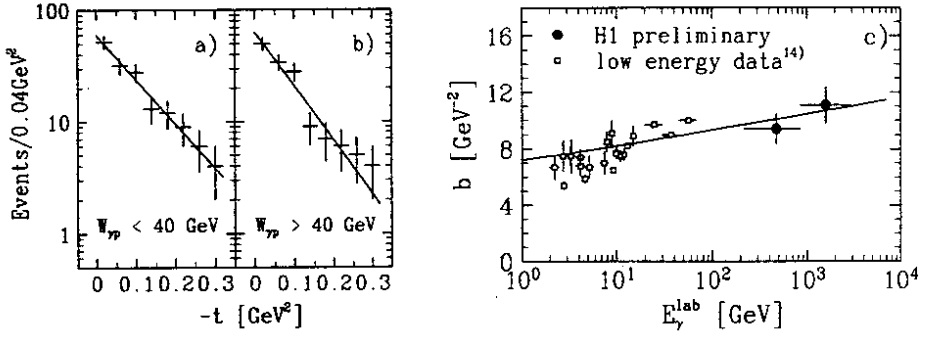

Figure 4: Slope of the elastic ρ^0 production. For the H1 data only statistical errors are shown. The line in fig. c) shows the phenomenological parametrization used in[2]

TRANSITION FROM SOFT TO HARD γp SCATTERING. For the inclusive particle distributions only charged tracks in the central region of $30° < \theta_{lab} < 150°$ and having $p_t > 0.3$ GeV/c were used. The total transverse energy in the event, E_T, was used as a measure of the 'hardness' of the γp interaction. Two parts have been selected from the whole e-tagged γp sample: 'soft' ($E_T < 5$ GeV) and 'hard' ($E_T > 10$ GeV). This selection was motivated by the Monte Carlo simulated events, using PYTHIA[12] with a $\hat{p}_t^{min}$ cutoff of 2.5 GeV/c for the hard γp scattering and low $p_\perp$ phase space Monte Carlo RAYPHOTON[15] for the soft γp scattering. The emphasis was put on getting 'hard' sample as clean as possible in order to be able to compare it with the QCD calculations, while the 'soft' one still may be contaminated by the medium $p_\perp$ events.

Fig. 5 shows, that the $p_\perp$ -distribution in the high E_T sample is described well by the PYTHIA Monte Carlo which included both direct and resolved photon contributions. The $p_\perp$ -distribution in the low E_T sample is a bit harder than the simple Monte Carlo, used in this case, predicts. Pseudorapidity distributions (fig. 5c) are very different for the two samples. Here only qualitative agreement with Monte Carli was observed. Note, that this distribution for the high E_T sample is sensitive not only to the photon structure function, but also to the scale of the hard process used (in our case it was $\hat{p}_t^2$). Finally, fig. 5d illustrates how the

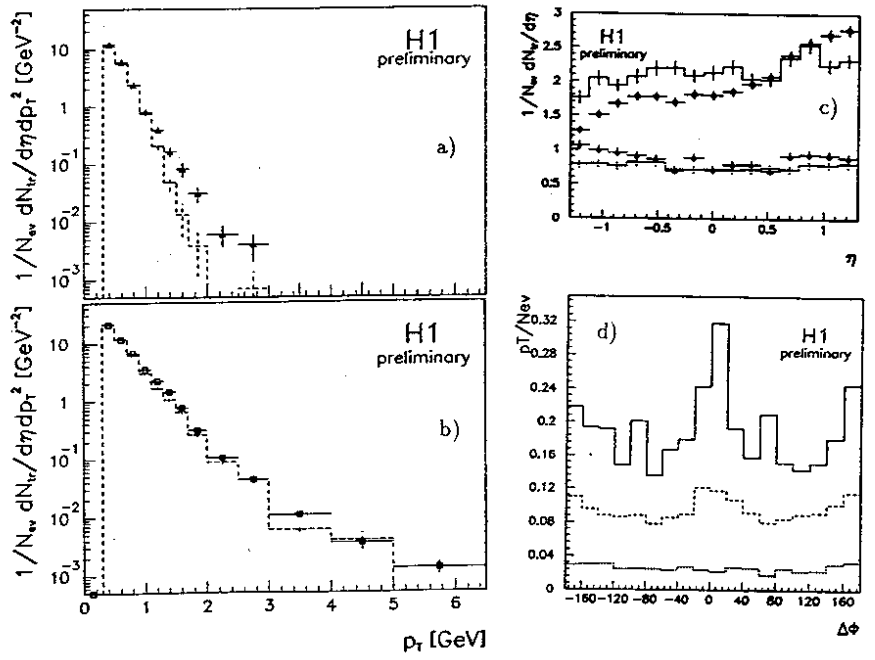

Figure 5: Inclusive $p_\perp$ spectra for the 'soft' (a) and 'hard' (b) γp events (points - data, histograms - MC); (c) pseudorapidity distributions for the 'soft' (triangles) and 'hard' (squares) samples compared to the Monte Carlo; (d) ϕ-distance to the highest $p_\perp$ particle in the event (dotted line - $E_T < 5$ GeV, dashed line - $E_T > 10$ GeV, solid line - $E_T > 20$ GeV)

event topology evolves with increasing E_T of the event: soft sample has no structure in the $\Delta\phi$-distribution, while for the $E_T > 20$ GeV particles clearly prefer two back-to-back cluster configuration ($|\Delta\phi| \simeq 0$ and $|\Delta\phi| \simeq \pi$), which is natural in case of jet production.

CONCLUSIONS. Already after the first months of operation at the level of few permille of the design luminosity, HERA has proven its great physics potential. New unexplored domains are opened both in deep inelastic scattering and photoproduction, and first interesting results have been obtained by H1 and ZEUS collaborations.

The γp total cross section has been measured at $\sqrt{s} \simeq 200$ GeV. No strong rise was observed, excluding some *extreme* minijet scenarios. The measurement is in good agreement with the Regge motivated parametrizations.

A clear ρ^0 signal is observed in the H1 detector. Both the angular distribution of the decay pions and the slope of the t-distribution show typical behaviour for the elastic scattering of transversly polarized photons: $\gamma p \rightarrow \rho^0 p$. The energy dependence of the elastic slope shows that the diffraction in γp interactions keeps shrinking at least up to $\sqrt{s} \simeq 80$ GeV.

Inclusive charged particle spectra demonstrate a transition from soft to hard γp scattering and the evidence of the jet formation in high-$E_\perp$ γp events.

REFERENCES

1) J.J.Sakurai, Ann.Phys. (N.Y.) **11** (1960) 1;
M.Gell-Mann and F.Zachariasen, Phys.Rev. **124** (1961) 953;
T.H.Bauer et.al., Rev.Mod.Phys. **50** 261.
2) G.A.Schuler and T.Sjöstrand, Phys.Lett. **B300** (1993) 169; CERN-TH.6796/93 (1993).
3) M.Erdmann, Momentum distributions of partons from resolved photons, these proc.
4) F.Brasse, The H1 detector at HERA, Proc. of the 26th Int.Conf. on High Energy Physics, Dallas (1992); H1 Collaboration, The H1 detector at HERA, to appear in NIM.
5) G.A.Schuler, Proc. of the Workshop on Physics at HERA, DESY (1992) 461;
A.Levy, ibid, 481; S.Levonian, ibid, 499.
6) ZEUS Collaboration, M.Derrick at al., Phys.Lett., **B293** (1992) 465.
7) H1 Collaboration, T.Ahmed et al., Phys.Lett., **B299** (1993) 374.
8) M.Drees and F.Halzen, Phys.Rev.Lett., **61** (1988) 275;
R.Gandhi and J.Sarcevic, Phys.Rev. D44 (1991) R10.
9) J.Sarcevic, Total and jet photoproduction at HERA, these proceedings.
10) A.Donnahie and P.V.Landshoff, Phys.Lett., **B296** (1992) 277.
11) H.Abramowicz et al., Phys.Lett., **B269** (1991) 465.
12) H.-U.Bengtsson and T.Sjöstrand, Comp.Phys.Comm., **46** (1987) 43;
T.Sjöstrand, Proc. of the Workshop on Physics at HERA, DESY, Hamburg (1991)1405.
13) R.Ross and V.Stodolsky, Phys.Rev., **149** (1966) 1172.
14) D.Aston et al., Nucl.Phys., **B209** (1982) 56 and references therein.
15) N.H.Brook, A. DeRoeck and A.T.Doyle, RAYPHOTON 2.0, Proc. of the Workshop on Physics at HERA, DESY, Hamburg (1991), Vol. 3, p. 1405.

Momentum Distribution of Partons from Resolved Photons

Martin Erdmann
Deutsches Elektronen Synchrotron
Notkestr.85, D-2000 Hamburg 52
H1 Collaboration

ABSTRACT

Jet events from photoproduction processes at HERA have been studied using the H1 detector. These enable the study of the quark and gluon content of the photon.

To appear in the proceedings of the session 'QCD and High Energy Hadronic Interactions' (20-27 March 1993)

Introduction: The study of the structure of the photon, using hard scattering processes involving quasi-real photons in the initial state, has been of interest for many years. It has been discovered that, in addition to it's pointlike nature, the photon can be considered as an object containing quarks and gluons.

At the electron-proton collider HERA the quasi-real photons are emitted by electrons scattering through very small angles. These photons are probed by the quarks and gluons of the protons. At high final state transverse momentum the formation of jets is observed, as reported in [1,2].

In leading order QCD the final state is characterized by 2 jets coming from the hard scattering process. The simplest diagrams are processes with the photon coupling directly to a quark from the proton, the so called *direct* photon processes (fig.1a), which include the QCD Compton and photon-gluon-fusion diagrams. The processes involving partons from the photon are usually refered to as *resolved* processes (fig.1b). In the kinematic region studied here the resolved processes exceed the direct ones by an order of magnitude. The momentum fraction which a parton from a resolved photon carries into the hard process can be approximately calculated using the transverse energy of the final state jets E_{t_i}, their polar angle Θ_i (wrt. the outgoing proton direction) and the energy of the photon E_γ:

$$x_\gamma \approx \frac{E_{t_1}\tan(\Theta_1/2) + E_{t_2}\tan(\Theta_2/2)}{2E_\gamma} \qquad (1)$$

In contrast to deep inelastic electron-photon scattering (fig.1c), which is due to the highly virtual photon of one of the leptons primarily sensitive to the quark content of the quasi-real photon of the other lepton, the photoproduction of jets from ep scattering probes both the quark and gluon content of the quasi-real photon. So far the momentum distribution of the gluons in the photon was not well experimentally constrained which lead to a variety of theoretical parametrizations for the structure function of the photon.

In this contribution we discuss high transverse momentum photoproduction events measured with the H1 detector. We look at a candidate event for a resolved photon process, show single jet cross sections in terms of transverse energy and rapidity and finally study the x_γ distribution with 2-jet events. The main emphasis is the access which HERA gives us to the quarks and gluons in the photon.

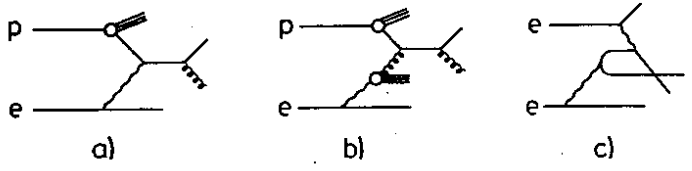

Figure 1: Examples of processes involving quasi-real photons: a) direct photon in ep-collisions, b) resolved photon in ep-collisions, c) deep inelastic electron-photon scattering in e^+e^- collisions.

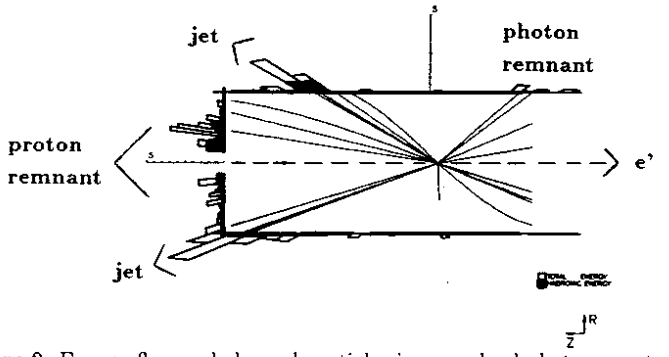

Figure 2: Energy flow and charged particles in a resolved photon event candidate.

Event candidate for a resolved photon process: In fig.2 a side view of an H1 event is shown. The hadronic and total energy deposited in the liquid argon calorimeter is displayed as are the charged particles detected in the tracking chambers. For a detailed description of the H1 detector refer to [3,4]. The proton enters from the right and the electron from the left, the direction of the quasi-real photon involved in the collision being essentially that of the electron. Around the beam hole to the left are visible energy deposits which may be due to the proton remnant, most of the energy of this will have disappeared down the beam pipe. Above and below the beam axis two jets are visible, probably the result of a hard scattering process. The scattered electron is detected in the luminosity system, not visible in the picture, and the remaining activity on the right side in the detector is probably due to the photon remnant.

Jets: The jets were found using a cone algorithm on a pseudo-rapidity $\eta = -\ln\tan(\Theta/2)$ and azimuthal angle Φ grid. The jet energy and direction were calculated with the definitions of the *snowmass accord* [5]. The jets were measured in the rapidity range $|\eta| \leq 1.5$ requiring a minimum transverse energy of $E_t \geq 7GeV$ in a cone of size $R = \sqrt{\Delta\eta^2 + \Delta\Phi^2} = 1$.

In fig.3 the differential inclusive jet ep-cross sections are shown in terms of the transverse energy and rapidity of the jets. With the scattered electron measured in the luminosity system the cross sections refer to a kinematic region of $Q^2 \leq 0.01GeV^2$ and $150 \leq W_{\gamma p} \leq 250GeV$, where Q^2 is the four momentum squared of the photon and $W_{\gamma p}$ is the invariant mass of the photon-proton system. The jet cross sections were corrected for detector effects and refer to particles measured in the cones. The inner error bars represent the statistical errors and the outer ones the statistical and systematic errors added in quadrature.

The curves in fig.3 were produced with the QCD generator PYTHIA [6] which is based on a leading order calculation for direct and resolved processes and includes initial and final state parton showers. For the proton structure function the GRV-LO [7] parametrization was used. Two different parametrizations of the photon structure function are shown, the full line is the prediction of GRV-LO [8] and the dashed line the prediction of the LAC-3 [9] parameterization. Note that the transverse energy distribution is mainly sensitive to the rate, while the rapidity distribution is also sensitive to the shape of the photon structure function. The LAC-3 structure

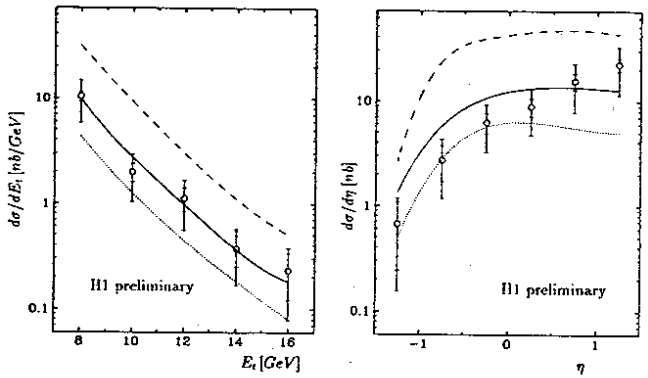

Figure 3: Inclusive jet cross sections in terms of transverse energy and rapidity. Points refer to H1 data, curves to leading order QCD calculations using the photon structure functions LAC-3 (dashed), GRV-LO (full) and GRV-LO excluding from the hard scattering gluons which originate from the photons (dotted).

function, which predicts many gluons at high x_γ, overshoots the data by a factor 2-3. The GRV-LO prediction is compatible with the data. The dotted line includes the direct photon processes plus the contribution of photons resolving into quarks (from GRV-LO). The latter is based on results from deep inelastic electron-photon scattering experiments. For central and negative rapidities these contributions are consistent with the data points, but at positive rapidities a gluon contribution is needed to describe the data.

Momentum fraction of partons: The momentum fraction x_γ of partons from resolved photons can be directly measured in 2-jet events using (1). The formula is mainly driven by the $\tan(\Theta/2)$ terms: for high x_γ one jet at large angle is sufficient, for low x_γ both jets should have small angles. In fig.4a the energy flow per event is shown versus the angle Θ (the scattered electron is not included here): low x_γ data (points) have more energy in the region $\Theta \approx 0°$ and less energy in the central region $\Theta \approx 90°$ compared to the measurements at high x_γ (triangles), which reflects the kinematics of the jets. For low x_γ only a small fraction of the photon energy enters the hard process, implying that much energy is left for the remnant. In the region $\Theta \approx 180°$ the low x_γ data overshoot the high x_γ data which we consider as a) confirmation of the existence of the photon remnant, and b) a demonstration that formula (1) is applicable.

In fig.4b the number of events with 2 jets is shown in terms of the parton momentum x_γ. Again a cone algorithm has been used allowing now for jets above a transverse energy of $E_t \geq 5GeV$ and a rapidity of $|\eta| \leq 2.5$. The distribution is shown above $x_\gamma = 0.2$ with statistical errors only. The data overshoot the kinematic limit $x_\gamma = 1$ due to the limited resolution in x_γ.

The curves in fig.4b were calculated with the PYTHIA Monte Carlo generator using the proton structure function MRSD0 [10]. The full and dashed lines are the results obtained with the GRV-LO and the LAC-3 photon structure functions as described above. The generated events were simulated with a detailed simulation program of the H1 detector and then reconstructed

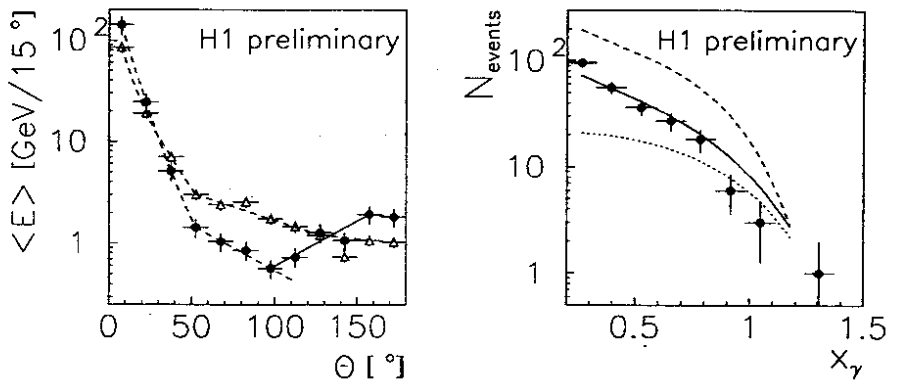

Figure 4: left: Energy flow per event for high x_γ (triangles) and low x_γ (points) data. The lines are merely to guide the eye. Right: Momentum fraction of partons from photons. Points are H1 measurements, curves are leading order QCD calculations as in fig.3.

with the same reconstruction program as used for the data. The normalization of the Monte Carlo events was determined using the measured luminosity ($23nb^{-1}$). The GRV-LO is, in this x_γ-range, compatible with the data, the LAC-3 predicts too many gluons. Recall that similar conclusions were drawn from the single jet rapidity cross section measurement. A correlation between the rapidity of a central jet and the x_γ of the event is expected from formula (1). Again, the difference between the full and dotted lines indicates the contribution of gluons originating from the photons of GRV-LO which is important in the region $0.2 \leq x_\gamma \leq 0.8$.

Summary: H1 has measured single jet cross sections for photoproduction events at HERA, which show sensitivity to the structure function of the photon. Analysis of 2-jet events enables determination of the momentum fraction which the partons from the photons carry into the hard scattering process. These photoproduction data are sensitive to the quark and the gluon content of the photon. A large amount of gluons in the photon at high x_γ, as predicted in the LAC-3 parametrization of the photon structure function, is not favoured by the data.

References:

1) T.Ahmed, et al, H1 collaboration, Phys.Lett. B297 (1992) 205
2) M.Derrick, et al, ZEUS collaboration, Phys.Lett. B297 (1992) 404
3) F.Brasse, DESY 92-140 (1992)
4) H1 Collab., *The H1 detector at HERA*, to be sub.to NIM
5) J.E.Huth et al, Fermilab-Conf-90/249-E
6) T.Sjöstrand, CERN-TH-6488 (1992)
7) M.Glück, E.Reya, A.Vogt, Z.Phys. C53 (1992) 127
8) M.Glück, E.Reya, A.Vogt, Phys. Rev. D46 (1992) 1973
9) H.Abramowicz, K.Charchula, A.Levy, Phys.Lett. B269 (1991) 458
10) A.D.Martin, W.J.Stirling, R.G.Roberts, Phys.Rev. D47 (1993) 867

Jets in Deep Inelastic Scattering at HERA

Hermann Küster
RWTH Aachen,
Sommerfeldstraße, D-5100 Aachen

H1 Collaboration

ABSTRACT

Jet rates in deep inelastic electron-proton scattering at HERA have been measured using the H1 detector. The expected variation of the multi-jet rates with the momentum transfer Q^2 was observed. Various QCD models, distinguished by their different treatment of parton emission, have been compared to our data.

To appear in the proceedings of the session 'QCD and High Energy Hadronic Interactions' (20-27 March 1993)

Introduction

Quantitative studies of jet production have so far been carried out extensively in e^+e^- and $p\bar{p}$ collisions. Recently, first evidence for multi-jet structure in fixed target deep inelastic μN scattering was reported [1]. Since May 1992, when the first electron-proton collisions were observed at the HERA storage ring, a new kinematic domain of deep inelastic scattering physics has become accessible experimentally. It is characterized by large hadronic masses, typically 100 GeV, and a large range of momentum transfer, from 5 GeV^2 to the kinematic limit of 10^5 GeV^2. The bulk of the present data is however at moderate momentum transfers ($< Q^2 > = 15$ GeV^2). This gives sufficient phase space for QCD parton emission to become clearly visible as distinct jets (see Fig. 1).

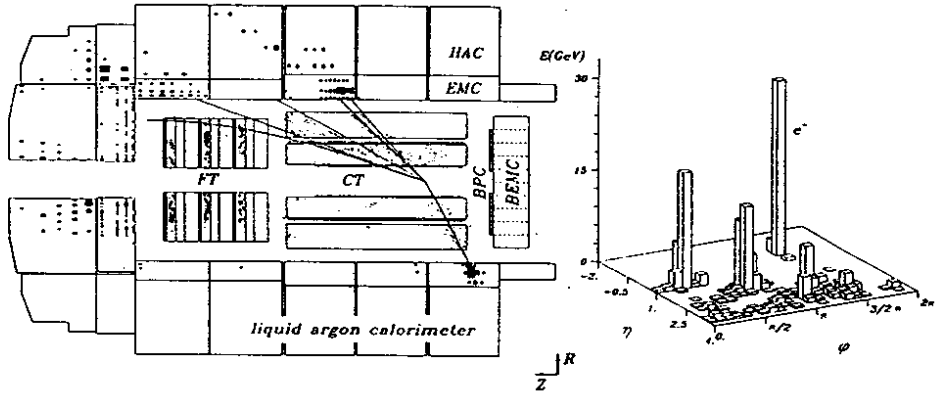

Figure 1: 2+1 jet event candidate, $Q^2 = 800$ GeV^2.

In the quark parton model (QPM), one jet arises from the struck quark scattering into the detector, while a second jet from the proton remnant generally escapes detection ("1+1" jet event, Fig. 2a). Due to QCD processes to $O(\alpha_s)$, such as gluon radiation in the initial or final state (QCD Compton, Fig. 2b+c) or photon-gluon fusion (Fig. 2d), a further jet appears, giving rise to 2+1 jet events. A

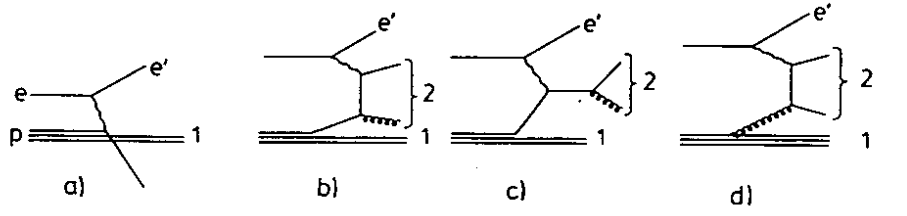

Figure 2: Processes giving rise to 1+1 (a) and 2+1 (b-d) jet events in deep inelastic scattering

first measurement of the hadronic final state in deep inelastic scattering of 26.7 GeV electrons and 820 GeV protons is reported in [2]. In the present contribution we concentrate on the measurement of jet rates in the hadronic final state. The data were collected in fall 1992 and amount to an integrated luminosity of about 24 nb^{-1}.

Event Sample

Fig. 1 shows a 2+1 jet event in the H1 detector. Two well separated jets are visible with a possible third jet close to the proton remnant direction. A detailed description of the H1 detector can be found in [3,4].

We consider events with the electron scattered into the backward calorimeter, labelled "BEMC" in Fig. 1, ($7° \lesssim \Theta_e \lesssim 23°$, $8\ \mathrm{GeV}^2 \lesssim Q^2 \lesssim 100\ \mathrm{GeV}^2$, "low Q^2" sample) and events with the electron scattered into the large LAr calorimeter ($\Theta_e \gtrsim 25°$, $Q^2 \gtrsim 100\ \mathrm{GeV}^2$, "high Q^2" sample). A cut in the scaling variable y is applied ($y < 0.5$ and $y < 0.6$ in the low and high Q^2 sample, respectively) in order to avoid regions in which QED corrections may be large. A cut on the hadronic invariant mass, $W^2 > 5000\ \mathrm{GeV}^2$, ensures substantial hadronic energy flow in the detector. The resulting data samples and their kinematic ranges are summarized in Tab. 1.

	low Q^2, 1100 events		high Q^2, 64 events	
	mean	range	mean	range
x	$1.5 \cdot 10^{-3}$	$10^{-4} - 10^{-2}$	$3 \cdot 10^{-2}$	$10^{-3} - 10^{-1}$
$Q^2\ [\mathrm{GeV}^2]$	15	8 – 100	520	> 100
W [GeV]	90	70 – 210	130	70 – 230

Table 1: Kinematic properties of the data sample used in the jet analysis

Jet Reconstruction

In deep inelastic scattering at HERA, the hadronic system is strongly boosted both along the beam direction and, to a lesser extent, transverse to it. Therefore, we make use of an (almost) Lorentz invariant cluster algorithm. The proton remnant is lost in the beam pipe. This is compensated in the jet algorithm by introducing a pseudoparticle carrying the missing longitudinal momentum of the event.

We use the JADE recombination scheme where the scaled invariant mass y_{ij} is defined as

$$y_{ij} = \frac{m_{ij}^2}{W^2}, \qquad \text{with} \qquad m_{ij}^2 = 2E_iE_j(1 - \cos\Theta_{ij})$$

neglecting the masses of cluster i and j. As scale we choose the invariant mass of the hadronic system W. Calorimeter cells are combined into clusters starting with the smallest invariant mass pair. Clustering is repeated until y_{ij} is above the jet resolution parameter y_{cut} for all clusters. The remaining clusters are counted as jets.

Jet reconstruction is based on calorimetric cells in the liquid argon and backward calorimeters covering a pseudorapidity interval of $-3.0 < \eta < 3.2$.

QCD models and Simulation

We compare our data to three different prescriptions for the simulation of QCD effects in deep inelastic scattering:

- Quark parton model and leading log parton showers as implemented in LEPTO 5.2 [5], labelled PS(WQ), and HERWIG 5.5 [6], labelled HERWIG,
- $O(\alpha_s)$ matrix element with matched parton showers as implemented in LEPTO 6.1 [7], labelled ME+PS, and
- the colour dipole model (ARIADNE 4.03 [8] as implemented in LEPTO 6.1), labelled CDM,

always using the MRS D0 [9] parton distribution functions for the proton.

The parton shower models have as a free parameter a scale determining the maximum virtuality in the parton shower and therefore the amount and hardness of gluon radiation. It has been shown in [2] that two possible extreme choices (namely Q^2 and W^2) fail to describe the hadronic final state. For LEPTO 5.2, in this study we have chosen an intermediate scale, $W \cdot Q$.

Jet Rates

We show uncorrected data on jet rates. Models are compared to data after a detailed simulation of the H1 detector and then reconstructed with the same reconstruction program as used for the

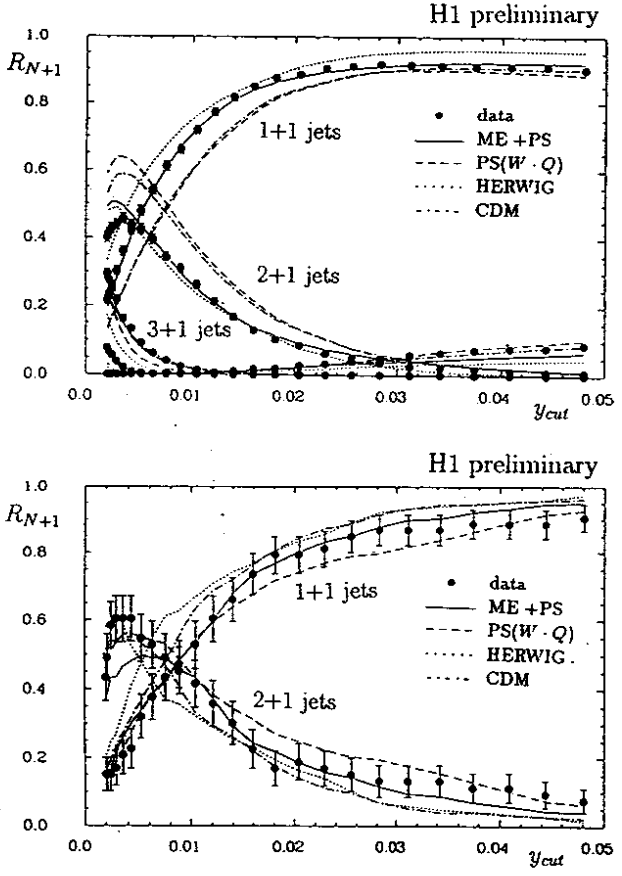

Figure 3: Fractional jet rates versus the jet resolution parameter y_{cut} for a) the low and b) the high Q^2 event sample compared to the predictions of different QCD models.

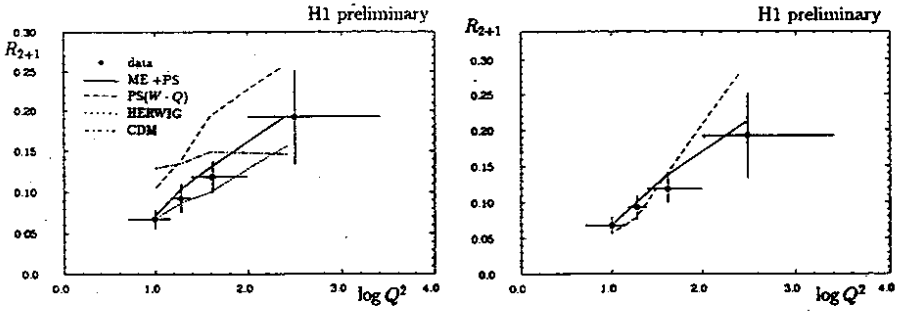

Figure 4: 3-jet rate versus momentum transfer Q^2 a) comparing different QCD model prediction and b) comparing the ME+PS model with a running (solid line) and constant (broken line) α_s.

data. Differences between jet rates at the level of partons, hadrons, and after detector simulation are moderate ($< 2\%$) for jet resolutions $y_{cut} \geq 0.02$.

Fig. 3a and 3b show fractional jet rates for 1+1, 2+1, and 3+1 jet events as a function of the jet resolution parameter y_{cut} for the low and high Q^2 sample respectively. Fixing the jet resolution parameter at $y_{cut} = 0.02$ corresponding to $m_{ij} > 10 - 30$ GeV yields a 3 jet fraction of $R_{2+1} = 9\% \pm 1\%$ ($20\% \pm 6\%$) in the low (high) Q^2 sample respectively (statistical errors only). The ME+PS model gives the best description of jet rates over the full range of y_{cut}, reproducing also the 4-jet rate. HERWIG gives a fair description, however the 4-jet rate is not properly described. Both PS(WQ) and CDM predict too high multi-jet rates.

Fig. 4a shows the fractional 3-jet rate as a function of the momentum transfer Q^2. We observe the expected rise with Q^2 due to the increased phase space for multi jet production. Both the ME+PS and the HERWIG model give a good description of the data, while PS(WQ) predicts a too high 3-jet rate and CDM fails to describe the rise with Q^2.

The rate of 3-jet events is proportional to α_s (c.f. Fig. 2b-d). Therefore, the Q^2 dependence of the 3-jet rate is sensitive to the Q^2 variation of α_s. Fig. 4b shows the 3-jet rate as function of Q^2 compared to the ME+PS model with a running α_s and a constant α_s. Although with the present data no discrimination is possible, it can bee seen that the slope of the Q^2 variation of the 3-jet rate is sensitive to the running of α_s.

Conclusions

At HERA, the hadronic system is strongly boosted and the proton remnant is not measurable. Nevertheless, jets and jet rates can be reconstructed reliably using a cluster algorithm. H1 has measured fractional jet rates as a function of the jet resolution parameter. They are well described by an $O(\alpha_s)$ M.E. model with matched parton showers. The 3-jet rate shows the expected rise with Q^2 and the Q^2 dependence of the 3-jet rate is sensitive to the variation of α_s with Q^2.

References

[1] E665 Collab., M.R. Adams et al. Phys. Rev. Lett. 69 (1992) 1026;
H. Melanson at this conference.

[2] H1 Collab., T. Ahmed et al., Phys.Lett. B298 (1993) 469.

[3] F. Brasse, Proceedings of the 26th International Conference on High Energy Physics, Dallas, 1992 and DESY preprint 92-140(1992).

[4] H1 Collab., "The H1 Detector at HERA", to be submitted to NIM.

[5] G. Ingelman, "LEPTO 5.2", unpublished program manual, see also
H.Bengtsson, G.Ingelman, and T.Sjöstrand, Nucl. Phys. B301 (1988) 554.

[6] G. Marchesini, B.R. Webber, G. Abbiendi, I.G. Knowles, M.H. Seymor, and L. Stanco, Comp.Phys.Comm. 67 (1992) 465, and references therein.

[7] G. Ingelman, "LEPTO 6.1", Proc. of the Workshop on Physics at HERA, eds. W. Buchmüller and G. Ingelman, Hamburg, 1991, vol. 3, 1366, and references therein.

[8] L. Lönnblad, ARIADNE version 4.03, Comp. Phys. Commun. 71 (1992) 15, and references therein.

[9] A.D. Martin, W.J. Stirling, R.G. Roberts, Durham preprint, DTP-92-16(1992);
H. Plothow-Besch, Proc. of the 3rd Workshop on Detector and Event Simulation in High Energy Physics, eds. K. Bos and B. van Eijk (NIKHEF-H, Amsterdam, 1991), p. 148 and CERN-PPE 1992.07.22.

FIRST MEASUREMENT OF THE PROTON F_2 STRUCTURE FUNCTION AT HERA

Claude Vallée
LPNHE Universités Paris VI et VII
4 Place Jussieu, Tour 33 RdC,
75252 Paris Cedex 05, France

ABSTRACT

We present the first measurement of the proton F_2 structure function performed by the H1 Collaboration at the HERA collider, using the full data sample accumulated in 1992. The kinematical domain presently accessible extends by two orders of magnitude down to low Bjorken x values ($x \sim 10^{-4}$) the region previously explored by fixed target deep inelastic scattering experiments. Preliminary results show a steeply rising F_2 which favours parton parametrisations based on a steep gluon x distribution already in this x range.

To appear in the proceedings of the session 'QCD and High Energy Hadronic Interactions'
(20-27 March 1993)

1. INTRODUCTION

In 1992, the HERA collider opened a new area in Deep Inelastic Scattering (DIS) by providing the first collisions of 26.7 GeV electrons and 820 GeV protons in the H1 and ZEUS detectors. The integrated luminosity accumulated by H1 amounts to 22.6 ± 1.6 nb^{-1} (5 % of which was the subject of a previous publication [1]) corresponding to about 1200 DIS neutral current events with a squared transferred momentum Q^2 between 8 and 100 GeV$^2/c^2$ and a Bjorken variable x down to 10^{-4}. This enables the measurement of parton distributions in a yet unexplored very low x domain where new effects like saturation and gluon recombination could become visible [2]. The present analysis is limited to the determination of the F_2 structure function, a quantity directly related to the measured differential cross-section.

2. DIFFERENTIAL CROSS-SECTION MEASUREMENT

In the present accessible kinematical domain, the topology of HERA DIS events is very similar to that of fixed target experiments: the deflection angle of the electron compared to its incident direction is relatively small and directly related to the Q^2 range of the event. The measurement of very low x events is determined by the ability to isolate low energy scattered electrons from the drastic HERA beam-gas and photoproduction background, whose dominant hadronic energy deposits may mimic fake electrons in the detector region surrounding the beam pipe. In contrast with fixed target experiments which measured only the scattered lepton, the HERA detectors provide a redundant access to x and Q^2 by measuring the hadronic jet issued from the scattered quark. This has triggered two independant approaches to the data analysis:

- a "detector oriented" approach, using only the electron energy E_e and angle θ_e, and computing the differential cross-section in the (E_e,θ_e) plane.
- a "physics oriented" approach dealing directly with the (x, Q^2) plane, where x is measured from a combination of the electron and hadron variables. This method requires a better understanding of the hadron measurement but as a counter part is less sensitive to initial state radiation corrections.

Both methods depend crucially on the backward part of the detector [3] where the scattered electron is identified and measured. Electron candidates are selected as a cluster in the Backward lead scintillator ElectroMagnetic Calorimeter ("BEMC") in coincidence with a track hit in the Backward Proportional Chamber. Background induced from upstream proton beam gas interactions is rejected through a veto on the Time of Flight scintillator plane located upstream the BEMC, as well as through a further requirement on the existence of a vertex in the interaction region. The photo-production background is cut through global kinematical constraints based on momentum conservation and through requirements on the electron cluster identification. The residual contamination is

measured from the luminosity electron tagger to be less than 1% globally and less than 10% at the lowest electron energy, set to 11 GeV in this analysis. The efficiency of all these selection criteria on DIS events is determined from the data themselves and amounts globally to 60%. The acceptance and smearing corrections depend mainly on the calibration of the BEMC, which is known within ± 2%. Efficiency and acceptance corrections are applied as multiplicative factors in the (E_e,θ_e) or (x,Q^2) plane to obtain the differential cross-sections.

3. F_2 DETERMINATION

The determination of F_2 from the differential cross-section requires in addition :

- a correction for initial state radiations, which amounts to up to 20 ± 10 % in our present highest Bjorken y region ($y \sim 0.6$).
- an assumption on the value of $R = \sigma_L/\sigma_T$, taken to be 0.5 as predicted by QCD for the parton parametrisation giving the best fit to our data (MRS D$^-$ [6]). This changes F_2 by at most 10 % compared to R = 0.

The resulting preliminary F_2 is shown in fig. 1 as a function of x at two values of Q^2. Systematic errors include uncertainties on the selection criteria efficiencies, acceptance corrections and radiation corrections. The global normalisation is known to ± 12 %. Both methods are in good agreement with each other and compatible with the results obtained at high x by the NMC [4] and BCDMS [5] Collaborations. Our measurement favours parton parametrisations assuming a steep behaviour of the gluon already in our x range (MRS D$^-$ [6] or GRV [8]) with respect to those based on a flat gluon x-distribution (MRS D0 [6] or CTEQ [7]). This conclusion should make the detection of saturation effects easier to achieve when larger statistics are available.

Acknowledgements

I am particularly indebted to all my colleagues of the H1 DIS analysis group for their combined effort in getting these results.

References

1) T. Ahmed et al, Phys. Lett. B 299 (1993) 385-393
2) L.V.Gribov, E.M.Levin, M.G.Ryskin, Phys. Rep. 100 (1983) 1
3) G. Cozzika, Proceedings of the 3rd International Conference on Calorimetry in High Energy Physics, Sept 29-Oct 2 1992, Corpus Christi, Texas
4) P.Amaudruz et al., Phys. Lett. B 295 (1992) 159
5) A.C. Benvenuti et al., Phys. Lett. B 223 (1989) 485
6) A.D.Martin, W.J.Stirling and R.G.Roberts, Durham preprint DTP-92-16 (1992)
7) J.Botts et al., Fermilab-Pub-92-371 (1992)
8) M.Glück et al., Z.Phys.C 48 (1990) 471

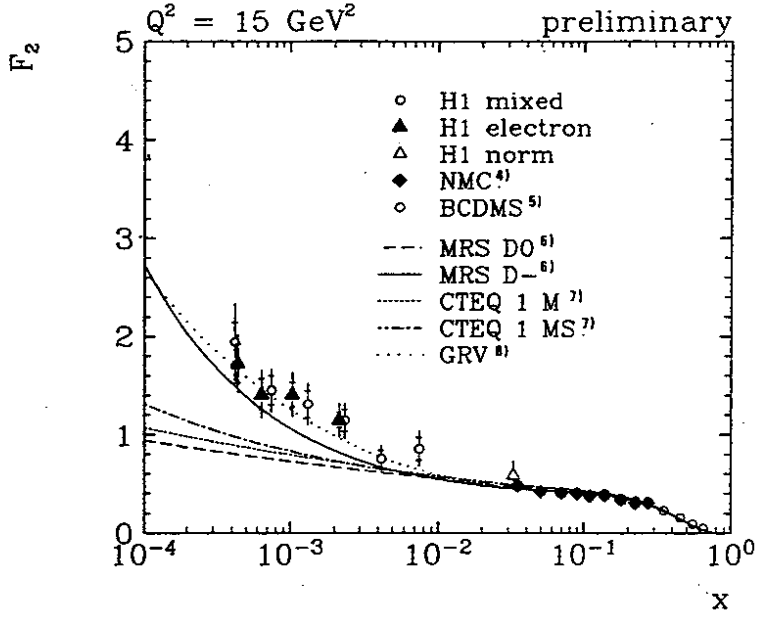

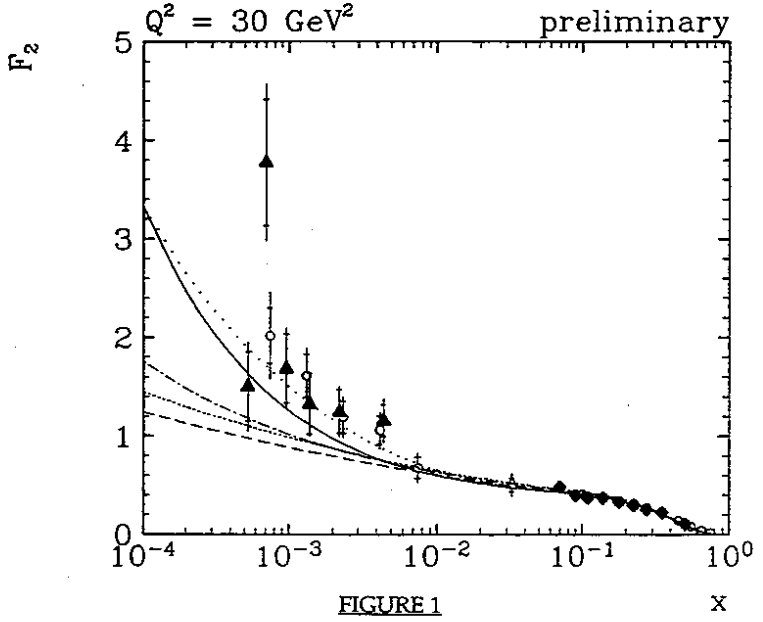

FIGURE 1

H1 preliminary F_2 compared to previous experimental results [4,5] and various parton parametrisations [6,7,8]

A Direct Search for New Particles in H1 at HERA

H1 Collaboration

Presented by Y. Sirois

LPNHE, Ecole Polytechnique, IN2P3-CNRS
Palaiseau, France

Abstract:

A search for new heavy particles in the H1 experiment at HERA is presented. Signatures of scalar and vector leptoquarks, leptogluons and excited leptons with flavours of the first generation were seeked for masses ranging from 35 GeV up to $\sim$ 250 GeV. No evidence for the production of such particles was found in various possible decay channels and rejection limits covering new mass-coupling domains are calculated. .

To appear in the proceedings of the session 'Electroweak Interaction and Unified Theory' (13-20 March 1993)

1 Introduction and Phenomenology

The discovery of heavy states beyond the particle spectrum of the $SU(3)\otimes SU(2)\otimes U(1)$ Standard Model of strong-electroweak interactions could provide guidance for an understanding of fundamental facts such as the quark-lepton symmetry or the existence of three generations of fermions and their mass spectrum. The ep collider HERA is ideally suited to look for leptoquarks, R-parity violating ($\not{R}_P$) squarks and leptogluons that could be produced as s-channel resonances between the incoming electron and a constituent of the proton. Excited leptons could also be singly produced via a resonance between the electron and a gauge boson radiated off the proton. This report presents a search [1] in H1 for direct single production of such particles based on $24 \pm 2\ \mathrm{nb}^{-1}$ of data collected at $\sqrt{s} = 296$ GeV in 1992.

Leptoquark bosons appear naturally, and possibly at accessible masses, in some grand unified theories [2], in superstring inspired models [3], in technicolour [4] and in some composite models [5]. Leptogluons are predicted in those composite models where the weak gauge bosons and the leptons are bound states of coloured constituents [6]. Squarks are bosonic partners of the quarks in supersymmetric models [7]. Excited states of known leptons are a natural ingredient of composite models [8]. In the narrow width approximation (and to lowest order), the production cross-sections for leptoquarks and leptogluons at HERA scale like $\sigma_{ep} \propto (\Gamma f(x)/M)$ where M is the mass of the heavy state. The term $f(x)$ denotes either the quark or the gluon density functions - as appropriate, and x is the standard scaling variable used in deep inelastic scattering (DIS). The widths Γ contain the model dependence on the couplings of the new particles. Similar formula holds for the production of excited leptons with f representing the number density of bosons radiated by the proton. The choice of a model will fix the possible decay channels and branching ratios into specific final states.

For leptoquarks: we consider first generation baryon and lepton number conserving scalar and vector bosons, having $SU(3) \otimes SU(2) \otimes U(1)$ invariant couplings to fermions, for which a most general effective Lagrangian was introduced in [9]. We assume mass degeneracy within each of the 10 allowed isospin families for which we adopt the nomenclature of [10]. Intergenerational mixing is considered forbidden [11]. The leptoquarks are only allowed to decay into fermions and may have sizeable Yukawa couplings λ only to either left or right handed leptons [11]. The partial decay widths are given [9] by $\Gamma_S = (\lambda^2/16\pi)\,M$ for scalar and $\Gamma_V = (\lambda^2/24\pi)\,M$ for vector leptoquarks. The production cross-sections are shown for $\lambda = 0.3$ in fig. 1. The isosinglet scalar S_0 appear in particular in superstring motivated E_6 models [3]. The $\tilde{S}_{1/2}$ which only couples to e-$\bar{d}$ has been proposed in a recent [12] extension of minimal $SU(5)$. The leptoquarks made by the "fusion" of an electron with an antiquark from the sea ($V_0, \tilde{V}_0, V_1, S_{1/2}$ and $\tilde{S}_{1/2}$) have cross-sections falling more steeply with mass than those which may involve valence quarks ($S_0, \tilde{S}_0, S_1, V_{1/2}$ and $\tilde{V}_{1/2}$). Initial state radiations dominate higher order QED corrections and lead to a relative suppression of the cross-sections at a given mass. Leptoquark events would be indistinguishable from standard DIS and consist (to lowest order) of a spectator jet from the proton remnant together with a lepton and a jet from the decay balancing each other in transverse momentum. They could nevertheless strikingly emerge on top of the DIS background as a narrow resonance centered at a mass $M \simeq \sqrt{x\,s}$. The separation could be further improved by exploiting the characteristic angular distribution of the decay products. The scalars decay isotropically in their center-of-mass frame yielding a flat $d\sigma/dy$ distribution where y is the standard scaling variable ($Q^2 = sxy$). The (polarized) vector leptoquarks would have $d\sigma/dy \propto (1-y)^2$. These distinguish from the steeply falling $\sim 1/y^2$ spectrum of DIS. **Squarks** in some $\not{R}_P$ supersymmetric models may have $\not{R}_P$ Yukawa

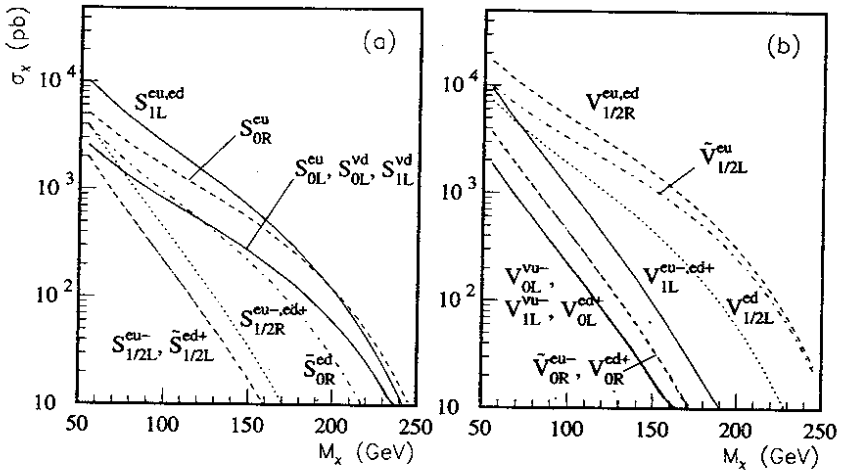

Figure 1: *Total cross-sections σ_X (at Born level) $\times$ branching ratio for $e + X$ and $\nu + X$ decay modes of ten leptoquark types in e^-p collisions at HERA. The label $S_{1L}^{eu,ed}$, for instance, designates the curve relevant for the production of an isotriplet scalar (S_1) of which two charge states have a non-vanishing coupling with left-handed (L) electrons.*

couplings λ'_L to e-q pairs only [7] and behave apparently like leptoquarks. The $\tilde{d}$ and $\tilde{u}$ can be produced in $e^- + u \to \tilde{d}$ and $e^- + \bar{d} \to \tilde{\bar{u}}$. and may decay via $\tilde{d} \to e^- + u$ or $\nu + d$ and $\tilde{\bar{u}} \to e^- + \bar{d}$, but the decays $\tilde{d} \to d + \tilde{\gamma}$ and $\tilde{\bar{u}} \to \bar{u} + \tilde{\gamma}$ via gauge couplings are expected to dominate [7]. The expression for the partial width of the $\not{R}_P$ decays is similar to that of scalar leptoquarks and one has the analogy that $\tilde{d} \sim S_0$ and $\tilde{\bar{u}} \sim \tilde{S}_{1/2}$. A possibility was discussed in [13] for a $\tilde{\bar{t}}$ (stop) to resemble the $\tilde{S}_{1/2}$ provided that a mass eigenstate of the stop exists which is lighter than the top quark and that the total decay width is dominated by $\not{R}_P$ decays.

For leptogluons: we consider a magnetic type coupling to electron-gluon pairs. The interaction Lagrangian for spin 1/2 electron-type leptogluon e_8 is taken [1] from [14] where chiral protection is imposed. The decay width is given by $\Gamma = \alpha_s M^3/4\Lambda^2$, where M is the leptogluon mass, Λ is a scale parameter and α_s is the strong coupling constant. Leptogluons $e + X$ signature is similar to that of some leptoquarks but they would have $d\sigma/dy \propto (1-y)$.

For excited leptons: lepton number conservation is imposed and we make use of an effective $SU(2) \otimes U(1)$ invariant Lagrangian [15] involving couplings for magnetic transitions between a spin 1/2 excited state (l^*) and an ordinary lepton (l). The l^* must have a chirality opposite to that of l and, more specifically, we assume that the excited electron (e^*) and neutrino (ν^*) form a weak doublet which couples only to the ordinary left handed (e, ν) doublet. The couplings are then explicitely given as $c_{\gamma e^* e} = -(f + f')/4$, $c_{\gamma \nu^* \nu} = (f - f')/4$, $c_{Z e^* e} = -(f \cot\theta_W - f' \tan\theta_W)/4$, $c_{Z \nu^* \nu} = (f \cot\theta_W + f' \tan\theta_W)/4$ and $c_{W \nu^* e} = c_{W e^* \nu} = f/(2\sqrt{2}\sin\theta_W)$ where θ_W is the weak mixing angle and f and f' are free parameters associated with the $SU(2)$ and $U(1)$ gauge groups. The e^* would be dominantly generated via the exchange of low Q^2 photons [16] whereas the ν^* would be formed at much higher Q^2 through

[1] This Lagrangian has been multiplied by 1/2 to be conform with the more common definition.

the interchange of a W gauge boson. The other couplings play a role in the decay. HERA allows for the first time the exploration of a mass range where the decay into heavy gauge bosons (W, Z) and a light fermion may become dominant. The partial decay widths are calculated [17] to be $\Gamma = (\alpha M^3 c^2_{\nu^* e} / \Lambda^2) \times (1 - M^2/M_V^2)^2(1 + M^2/2M_V^2)$ for a decay involving a given vector boson V. The branching ratios are approximately constant at large masses $(M/M_{W,Z})^2 \ll 1$

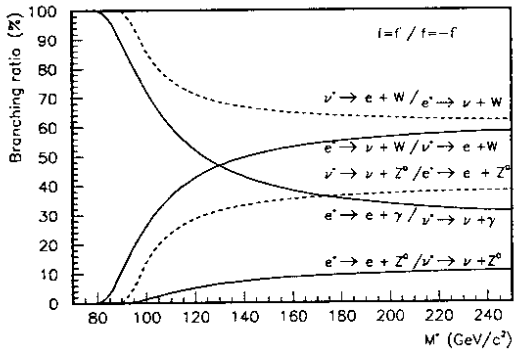

Figure 2: *Branching ratios (in %) of the three decay channels for the excited electron and neutrino for f=f'=1 and for f=$-f'$=1.*

and depend crucially on the value of the free parameters f and f' as seen for example in fig. 2 which stresses the complementary role of the e^* and ν^* searches. In this paper, all semi-leptonic decay modes listed in fig. 2 are considered. In cases where a W or Z boson is involved, the analysis is restricted to its purely leptonic decay modes (with flavours of the first or second generation) and at least one electron must be present in the observable final state; e.g. in the case $e^* \to \nu W^-$, only the $W^- \to e^-\bar{\nu}$ (branching ratio $\mathcal{B} \approx 10\%$) is considered while in the case $\nu^* \to e^- W^+$, both the $W^+ \to e^+\nu$ and $W^+ \to \mu^+\nu$ modes are treated. Conversely, in the $\nu^* \to \nu Z$ mode, only the $Z \to e^+e^-$ ($\mathcal{B} \approx 3.3\%$) is considered while in the case $e^* \to e^- Z$, all $Z \to e^+e^-$, $Z \to \mu^+\mu^-$ and $Z \to \nu\bar{\nu}$ ($\mathcal{B} \approx 20\%$) are treated.

2 Search for Leptoquarks, Leptogluons and Squarks

For searches in the $e + X$ final states, the events are required to have been registered via total or transverse energy triggers based on liquid argon (LAr) calorimetry measurements. The LAr calorimeter modules [18] cover $4° \leq \theta \leq 155°$ (with θ defined from the proton beam direction) and measure electron energies in lead/argon electromagnetic (e.m.) sections with a resolution of $\sigma(E)/E \simeq 11\ \%/\sqrt{E}$ (E in GeV) and hadron energies [19] together with stainless-steel/argon sections with $\sigma(E)/E \simeq 50\%/\sqrt{E}$. A reconstructed electron candidate with $E_T^e > 10$ GeV must be found at $\theta_e > 10°$ whereby a candidate is a cluster of LAr cells having 90% of its energy in the e.m. section. The electron must be isolated in the sense that there should be less than 10% additional hadronic energy and no muon track or energy (i.e. < 1 GeV) in an iron yoke (instrumented with layers of streamer tube chambers and surrounding the LAr calorimeter) within a cone of azimuthal angle ϕ and pseudorapidity η of opening $\sqrt{(\Delta\eta)^2 + (\Delta\phi)^2} < 0.5$ centered on the candidate and viewed from the (required) reconstructed interaction vertex. Finally, we require a matching between the y_e scaling variable measured with the electron and y_h measured via the hadronic flow, $| y_e - y_h | < 0.3$ with $y_e = 1 - (E_e - P_{z,e})/2E_e^\circ$ and $y_h = (E_h - P_{z,h})/2E_e^\circ$; where the subscript h denotes the

sum over all particles measured in the LAr calorimeter excluding the electron candidate; E_e° and E_p° are the incident electron energy (26.7 GeV) and the proton energy (820 GeV). The remaining event sample was visually scanned and one further cosmic muon event was identified and rejected. The high E_T^e requirement suppresses strongly the background from photoproduction while maintaining a high efficiency for the resonance search for which a Jacobian peak at $E_T^e \approx M/2$ is expected. The isolation requirements and the Δy cut mainly rejects misidentified photoproduction events. The Δy cut also rejects events where a hard undetected photon was radiated from the initial state electron. The required absence of energy flow in the instrumented iron suppresses contamination from cosmic muon induced showers. For the searches in the $\nu + X$ final states, we require a missing transverse momentum of $P_T^{miss} \equiv \sqrt{(\sum E_x)^2 + (\sum E_y)^2} > 20$ GeV measured by the calorimeters. Events with an electron candidate (as defined above) with $E_T^e > 10$ GeV are rejected. Five events with clear cosmic induced patterns (punch through muon tracks) were rejected at a visual scanning.

For an $e + X$ event, the resonance mass is calculated using $M = \sqrt{s x_e}$ where x_e is obtained from the measured electron as $x_e = E_e E_e^\circ \cos^2\frac{\theta_e}{2} / \left(E_p^\circ \left[E_e^\circ - E_e \sin^2\frac{\theta_e}{2}\right]\right)$. This mass determination is well suited at large y, our region of interest. For a $\nu + X$ event candidate, the mass is calculated via $M = \sqrt{s x_h}$ where x_h is computed from the measured hadronic energy flow as $x_h = (P_{T,h}^2)/(1 - y_h)\ y_h\ s$. After all selection cuts, 43 $e + X$ events remain with reconstructed 'leptoquark' masses above 35 GeV. In these events, the electron E_T, which reaches ~ 50 GeV, is very well correlated with the total E_T and $E_T^e/E_T^{total} \sim 45\%$ as expected given the broadening of the jet caused by parton shower and fragmentation effects. One $\nu + X$ event with a $P_T^{miss} = 37$ GeV remains in this mass domain showing the expected signature of a high P_T current jet together with the energy flow from the proton remnant. The calculated mass of this $\nu + X$ candidate is 93 GeV.

The remaining data sample are compared to Monte Carlo predictions for DIS from the DJANGO event generator [20], folding in trigger efficiencies, monitored by using track triggers. The measured P_T^{miss} is compared to the DIS event simulation in fig. 3 (a). The events are well balanced in the transverse plane and the Monte Carlo reproduces well the tail of the P_T^{miss} distribution which is mainly due to detector resolution and energy losses. The mass distribution is shown in fig. 3 (b) before and after a final kinematical cut of $y_e > 0.25$. This cut was chosen as a compromise to optimise the signal-to-background ratio for scalar leptoquark searches while maintaining efficient detection of vector leptoquarks. It also safely rejects the low y region where both y_e and x_e are badly measured. Both the absolute number of events and the shape of the mass spectra are well reproduced by the simulation before and after the y_e cut. For the $\nu + X$ final states, no additional kinematical cuts are applied and a mean number of 0.66 charged current events are predicted by the Monte Carlo simulation after folding in the LAr trigger efficiencies for the hadronic flow. The data samples being compatible on an absolute scale with expectations from standard DIS background, we derive rejection limits under the hypothesis that all observed events originate from such background.

To compute efficiencies for the various leptoquark types or for leptogluons we make use of the COMPOS event generator [10]. The leptoquarks or leptogluons are not fragmented before decay. Such a crude approximation is justified if one considers that leptoquarks and leptogluons may have 'hard' fragmentation functions not unlike those of heavy quarks. For leptoquarks, the contribution (available in [10]) of the interference with DIS diagrams in a mass bin centered on the resonance is small and henceforward neglected. The mass resolutions $\sigma_{S,V}$ roughly scale linearly with mass at small coupling values (e.g. $\lambda \lesssim 0.3$) where the intrinsic width of the resonance is small compared to detection resolution. We find that $\sigma_S \simeq 1.6$ GeV

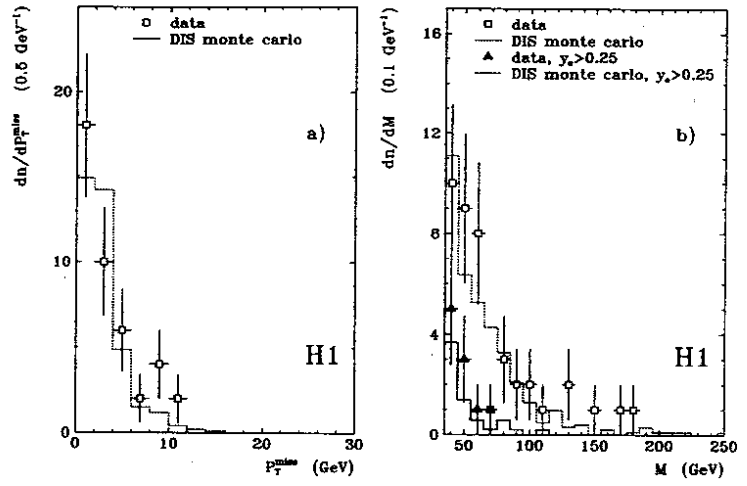

Figure 3: *P_T^{miss} distribution (a) and mass spectrum (b) for $M > 35$ GeV before (open points) and after (closed points) a cut on y_e. The histogram curves show the absolute prediction of a DIS Monte Carlo simulation before (dashed) and after the (solid) y_e cut.*

at $M = 50$ GeV ($\simeq 2.5$ GeV at $M = 150$ GeV) for scalars and $\sigma_V \simeq 2.4$ GeV at 50 GeV ($\simeq 3.3$ GeV at 150 GeV) for vectors in the $e + X$ decay channels while in the $\nu + X$ channels we find $\sigma_S \simeq 8.6$ GeV at $M = 50$ GeV ($\simeq 13.5$ GeV at $M = 150$ GeV) and $\sigma_V \simeq 6.1$ GeV at 50 GeV ($\simeq 11.0$ GeV at 150 GeV). The vector leptoquarks are concentrated towards lower y_h where the resolution on x_h improves. For leptogluons, the mass resolutions are $\sigma_{\tilde{e}_8} \simeq 1.5$ GeV at $M = 50$ GeV and $\simeq 3.2$ GeV at 150 GeV. The efficiency losses are mainly due to the kinematical cut on y_e for $e + X$ final states and to trigger efficiency. An overall loss factor of $\approx 85\%$ is conservatively included in the overall detection efficiency to account for the fact that all the relevant hardware triggers were simultaneously operational for that fraction of the integrated luminosity. Besides that overall factor, the detection efficiencies integrated within $[M \pm 3\sigma]$ (including losses from selection and kinematical cuts as well as other trigger losses) for scalar leptoquarks in the mass range from 100 to 200 GeV is $\approx 60\%$ in the $e + X$ decay mode and $\approx 70\%$ in the $\nu + X$ mode. In the same mass range, the efficiencies for vector leptoquarks is $\approx 35\%$ in the $e + X$ decay mode and $\approx 65\%$ in the $\nu + X$ mode. For leptogluons in this mass range, the detection efficiency is $\approx 45\%$.

Integrating the background in $[M \pm 3\sigma_{S,V}]$ moving mass windows centered on nominal M values, we calculate cross-section limits for scalar and vector leptoquarks and derive coupling limits for all leptoquarks. Whenever relevant, neutral and charged lepton decay modes are combined. The results in the mass-coupling plane are shown in fig. 4. For $\lambda = 0.3$ which corresponds to an electromagnetic coupling, i.e. $\alpha = \frac{\lambda^2}{4\pi}$, the mass limits at 95% CL are $M > 181\,(S_0^L)$, $178\,(S_0^R)$, $145\,(\tilde{S}_0^R)$, $192\,(S_1^L)$, $152\,(V_{1/2}^L)$, $190\,(V_{1/2}^R)$ and 183 GeV $(\tilde{V}_{1/2}^L)$ for leptoquarks resulting from electron fusion with quarks and $M > 98\,(V_0^L)$, $102\,(V_0^R, \tilde{V}_0^R)$, $121\,(V_1^L)$, $98\,(S_{1/2}^L, \tilde{S}_{1/2}^L)$ and 112 GeV $(S_{1/2}^R)$ in case of a fusion with antiquarks. We have therefore improved on the current limits from $p\bar{p}$ experiments after only a few months data taking on HERA (for the S_0^L (S_0^R) which has $\mathcal{B} = 50\%\,(100\%)$ into $e + X$, the CDF limit [21] at 95% CL is 82 GeV (113 GeV) almost independently of the coupling λ). It should be noted that a

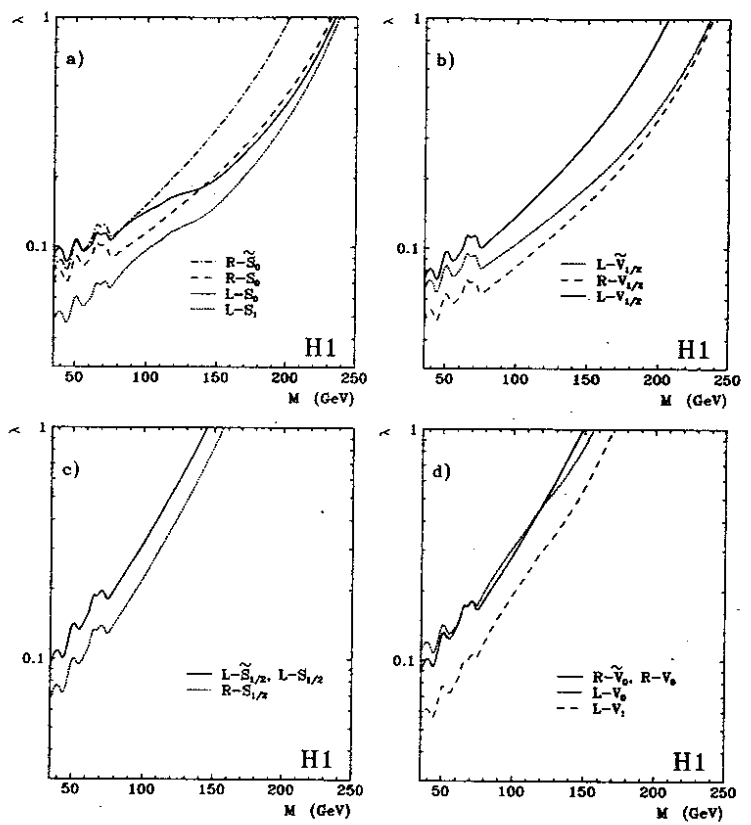

Figure 4: *Rejection limits at the 95% CL for the coupling $\lambda_{L,R}$ as a function of mass for scalar and vector leptoquarks with fermion number F=2 (a), (b) and F=0 (c), (d). The regions above the curves are excluded. The limits on λ_L for S_0, S_1, V_0 and V_1 combine charged and neutral decays.*

model dependant indirect limit of $\lambda_L \lesssim M/1.7$ TeV has been derived [11] from the universality of the Fermi constant measured in μ decays and β decays. The coupling limits for $\tilde{S}_{1/2}$ may also be interpreted as limits on the stop of R_P supersymmetry [13]. There is an uncertainty on the coupling limits due to ambiguities in the structure function used in the calculation of leptoquark cross-sections. By comparing the results of fig. 4 obtained using the MT-B1 parametrisation with those obtained using MT-B2, MRS-D0 and D− [22], the systematic deviations on the limits are found to amount to 7% for leptoquarks coupling to quarks and to 12% for those interacting with anti-quarks. For the QCD scale at which quark densities are evaluated we chose Q^2. Alternative choices like P_T^2 and M^2 yield an additional uncertainty of 7%.

For leptogluons, the limits in the Λ^{-1} versus $M_{\tilde{e}_8}$ plane are shown in fig. 5. We exclude at 95% CL scale parameters $\Lambda \lesssim 1.8$ TeV for a leptogluon at $M \simeq 100$ GeV and $\Lambda \lesssim 200$ GeV at

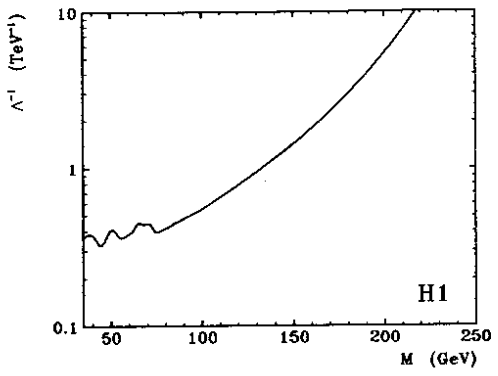

Figure 5: *Rejection limits at the 95% CL for the inverse of the scale parameter* Λ *versus* M *for* e_8 *leptogluons. Values above the curve are excluded.*

$M \simeq 200$ GeV. This improves on existing indirect limits of $M_{e_8} \times 4\Lambda^2 \gtrsim (240\ \text{GeV})^3$ derived by JADE [23, 14]. A direct limit of $M \gtrsim 110$ GeV from pair production via colour gauge interactions is derived from $p\bar{p}$ collider data [24].

3 Search for Excited Leptons

All observable final states considered here for the e^* and ν^* searches are characterized by one or more energetic e.m. clusters accompanied, in some channels, by one or more muons and/or missing energy. The muons are measured in an instrumented iron covering $5° \leq \theta \leq 170°$ and in a forward muon spectrometer in the region $3° \leq \theta \leq 17°$. For cases with only one electron or one photon, the event candidates are required to have at least one isolated LAr e.m. cluster with $E > 15$ GeV and a large overall momenta imbalance $P_T^{miss} > 16$ GeV. This suppresses the background from low Q^2 DIS. In the $e^* \to e\bar{\mu}\mu$ channel, the requirement on the e.m. cluster is loosen to $E > 5$ GeV and at least one of the two muons must be found outside the forward muon spectrometer. This suppresses the contamination from misidentified proton beam induced hadronic background and as well as most beam halo muons. For the channels with two e's or with one e and one γ, two LAr e.m. clusters with $E > 30$ GeV and 15 GeV respectively are required and one of those must be found at $\theta \gtrsim 15°$. The requirement that both e.m. clusters be found in the LAr calorimeter strongly suppresses Compton scattering ($ep \to e\gamma p(X)$) background. In the $e^* \to e^-e^+e^-$ case, the three isolated clusters must each have $E > 10$ GeV and at least two of them must be at $\theta > 10°$. The event candidates of the various channels were visually scanned and events clearly identified has contamination from showering cosmic and halo muons were rejected. The above mentioned cuts were optimized for e^* and ν^* searches at large masses and no candidates are left in the region of interest $M \gtrsim 75$ GeV. This is possible considering the background expectations in the various channels. For example, using the formulae of [25], we expect less than 0.1 events for invariant $e\gamma$ masses above 75 GeV from the Compton process which is the dominant background for the classes with two e.m. clusters.

In absence of any e^* or ν^* signal we derive rejection limits. The detection efficiencies as function of mass in the various channels are determined using of the event generator COMPOS [10] which implements the cross-section calculated in [15], and folding in trigger efficiencies for the specific e.m. cluster analysis determined from data triggered by cosmic and halo

muons. The trigger efficiency for the $e^* \to e\mu\mu$ channel is obtained from Monte Carlo studies including a full simulation of the muon trigger. Typical values for the detection efficiencies are of about 80 % in the mass range $M \gtrsim 100$ GeV. The rejection limits are calculated on the product $c_{V l^* l} \times \Lambda \times \sqrt{B}$ where B was given in fig. 2. These limits are shown in fig. 6 for different decay channels as a function of mass. The curves cover mass-coupling values for

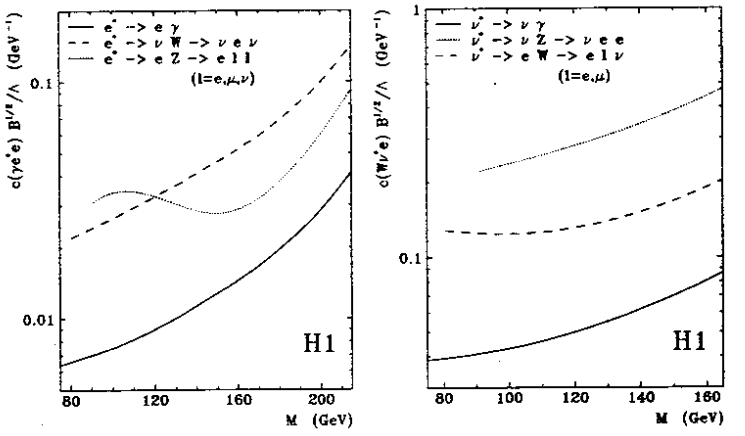

Figure 6: *Rejection limits at the 95% CL for the three decay modes of the* e^* *and* ν^*. *Regions above the curves are excluded.*

which the decay width is much smaller than the mass (e.g. $\Gamma \lesssim 30$ GeV at $M_{e^*} = 215$ GeV or $M_{\nu^*} = 165$ GeV for $f = 0$, $f' = 1$). We find at 95% CL for example at $M = 100$ GeV that $c_{\gamma e^* e}\sqrt{B}/\Lambda \gtrsim 7 \times 10^{-3}$ GeV^{-1}. The dominant uncertainty on the coupling limits comes from the choice of the proton structure functions and is estimated to be of the order of 10%. The best current rejection limits for the direct single production of excited leptons were obtained by LEP experiments [26] in the $l + \gamma$ decay mode and exclude masses $M_{e^*} \lesssim 90$ GeV almost independently of the composite scale Λ for $\Lambda \lesssim 2.5$ TeV. In the scattering process $e^+e^- \to \gamma\gamma$ indirect limits [26] for $c_{\gamma e^* e}\sqrt{B}\,/\,\Lambda$ are of $O(10^{-2})$ GeV^{-1} for masses of $O(100)$ GeV.

4 Conclusions

We have searched with the H1 detector for direct production of scalar and vector leptoquarks, leptogluons, excited electrons (e^*) and excited neutrinos (ν^*) in a mass range not accessible directly at other existing colliders. No evidence was found for the production of leptoquarks with any possible $SU(2) \otimes U(1)$ multiplet assignments and coupling limits were calculated as a function of mass. For a coupling value of $\lambda = 0.3$ we obtain mass limits at 95% CL ranging from $M \gtrsim 145$ GeV to 192 GeV for leptoquarks resulting from the fusion of an electron and a quark and from $M \gtrsim 98$ to 121 GeV for leptoquarks formed with an antiquark. No evidence for leptogluons was found and at 95% CL the scale values $\Lambda \lesssim 1.8$ TeV are excluded for $M \simeq 100$ GeV. The e^* and ν^* were searched in several decay modes. No direct evidence was found for their production and coupling limits on couplings were presented.

Acknowledgements

The H1 Collaboration is very grateful to the DESY technical staff and to the H1 engineers and technicians. I wish to thank all members of the H1 Collaboration for their support.

References

[1] The H1 results on new particle searches were recently discussed in:
H1 Collab., Nucl. Phys. B396 (1993) 3.
[2] J.C. Pati and A. Salam, Phys. Rev. D10 (1974) 275; P. Langacker, Phys. Rep. 72 (1981) 185; G. Senjanović and A. Šokorac, Z. Phys. C20 (1983) 255.
[3] V.D. Angelopoulos et al., Nucl. Phys. B292 (1987) 59; A. Dobado, M.J. Herrero and C. Muñoz, Phys. Lett. B191 (1987) 447.
[4] S. Dimopoulos, Nucl. Phys. B168 (1980) 69; E. Farhi and L. Susskind, Phys. Rev. D20 (1979) 3404.
[5] B. Schrempp and F. Schrempp, Phys. Lett. B153 (1985) 101, and references therein.
[6] H. Fritzsch and G. Mandelbaum, Phys. Lett. B102 (1981) 319.
[7] J. Butterworth and H. Dreiner, Nucl. Phys. B397 (1993) 3.
[8] M.E. Peskin, Proc. of the Xth Sympos. on Lepton-Photon Interact., Bonn (1981) p 880.
[9] W. Buchmüller, R. Rückl and D. Wyler, Phys. Lett. B191 (1987) 442.
[10] T. Köhler, Proc. of the Workshop Physics at HERA, DESY, Hamburg (October 1991) Vol. 3 p 1526 (COMPOS version 1.4).
[11] W. Buchmüller and D. Wyler, Phys. Lett. B177 (1986) 377; O. Shanker, Nucl. Phys. B204 (1982) 375; Ibid., B206 (1982) 253.
[12] H. Murayama and T. Yanagida, Tohoku U. preprint TU-370 (May 1991).
[13] T. Kon and T. Kobayashi, Phys. Lett. B270 (1991) 81.
[14] J. Bijnens, Proc. of the 1987 HERA Workshop, DESY, Hamburg (October 1987) Vol. 2 p 819; K.H. Streng, Z. Phys C33 (1986) 247.
[15] K. Hagiwara, S. Komamiya and D. Zeppenfeld, Z. Phys. C29 (1985) 115; F.E. Low, Phys. Rev. Lett. 14 (1965) 238; F.M. Renard, Phys. Lett. B116 (1982) 264; F.M. Renard, Phys. Lett. B126 (1983) 59.
[16] A. Courau and P. Kessler, Phys. Rev. D33 (1986) 2028.
[17] J. Kühn and P. Zerwas, Phys. Lett. B147 (1984) 189.
[18] A description of the H1 detector can be found in: G. Cozzika, Proc. IIIrd Int. Conf. on Calorimetry in H. E. P., Corpus Christi, (1992).
[19] B. Andrieu et al., H1 Calorimeter Group, DESY preprint 93-047 (April 1993).
[20] G.S. Schuler and H. Spiesberger, Proc. of the Workshop Physics at HERA, DESY, Hamburg (October 1991) Vol. 3 p 1419 (DJANGO version 1.0), and references therein.
[21] S.M. Moulding, CDF Collab., Fermilab preprint CONF-92-341-E (November 1992).
[22] A.D. Martin, W.J. Stirling and R.G. Roberts, Durham preprint, DTP-92-16 (1992); J. Morfin and W.K. Tung, Z. Phys. C52 (1991) 13.
[23] JADE Collab., Z. Phys. C36 (1987) 15.
[24] U. Baur and K.H. Streng, Phys. Lett. B162 (1985) 387.
[25] F. Raupach, Proc. of the Workshop Physics at HERA, DESY, Hamburg (October 1991) Vol. 3 p 1473; A. Courau and P. Kessler, Phys. Rev. D46 (1992) 117.
[26] ALEPH Collab., Phys. Rep. 216 (1992) 253; L3 Collab., Phys. Lett. B288 (1992) 404; Ibid., B252 (1990) 525; OPAL Collab., Phys. Lett. B257 (1991)531; Ibid., B244 (1990) 135; DELPHI Collab., Z. Phys. C53 (1992) 41; Idem, Phys. Lett. B268 (1991) 296.